Mitotic bypass and continued endocycling promote cancer cell survival after genotoxic chemotherapy

Kevin Truskowski[1, 2], Louis Rolle[1], George Butler[1, 3], Margaret E Yang[1], Kenneth J Pienta[1, 2], Sarah R Amend[1, 2]

Corresponding Authors:

Kevin Truskowski; ktrusko1@jhmi.edu

Sarah R Amend; samend2@jhmi.edu

Affiliations:

1. Cancer Ecology Center, The Brady Urological Institute, Johns Hopkins School of Medicine, Baltimore, MD 21287, USA.
2. Cellular and Molecular Medicine Graduate Program, Johns Hopkins School of Medicine, Baltimore, MD 21287, USA.
3. University College London, Cancer Institute, London WC1E 6DD, UK.

Abstract

Genotoxic chemotherapies are central components of the treatment regimen for most cancers but are rarely curative. Drug-tolerant persister cells (DTPs) evade cell death during these treatments by accessing transient adaptive states and can contribute to cancer progression after treatment. Here, we demonstrate that cancer cells can survive genotoxic chemotherapy-induced stress by accessing a DTP state wherein stress-induced bypass of mitosis precipitates continued endocycling which promotes survival by allowing cells to evade mitotic catastrophe and cell death. Mechanistic studies indicate that persistent DNA damage signaling in endocycling persister cells triggers sustained p53-independent CDK1 inhibition by WEE1 and Myt1. Continued survival in endocycling persisters is dependent on activation of this G2 checkpoint, and disrupting WEE1 or Myt1 activity using clinical-stage small molecule inhibitors is sufficient to drive CDK1 reactivation, forcing mitotic entry, catastrophe, and cell death. Our results define endocycling DTPs as targetable mediators of cancer cell persistence after genotoxic therapy.

31 **Introduction**

32 Genotoxic chemotherapies are central tools for the treatment of most cancers.
33 These drug regimens commonly induce initial tumor regression but leave behind surviving
34 populations that can seed relapse. Understanding which cancer cells survive treatment
35 and how they do so remain urgent questions for the field. Resistance to chemotherapy
36 has largely been attributed to models of genetic heterogeneity whereby a subpopulation
37 of cells harboring a preexisting genetic advantage is selected for under therapeutic
38 pressure, expands, and becomes the dominant population in the recurrent tumor. While
39 evidence supporting this model is plentiful, it has become clear that non-genetic
40 mechanisms of resistance are also common[1]. In lieu of genetic advantage, drug-tolerant
41 persister cells (DTPs) survive drug treatment by accessing transient adaptive states and
42 are increasingly recognized drivers of cancer lethality[2-4]. DTPs have been described in
43 various cancer models, including lung, pancreatic, prostate, breast, and melanoma, and
44 in response to both targeted therapies (e.g., kinase inhibitors) and cytotoxic drugs (e.g.,
45 platinum-based chemotherapy)[3]. Cancer cells' rapid adaptation to diverse stressors
46 highlights the significance of these states in determining treatment outcome.

47 Chemotherapy treatment classically induces cell death or cell cycle arrest. In
48 addition to these, it is also well understood that stress signals downstream of telomere
49 damage[5], replication stress[6], ribotoxic stress[7], among others, can trigger premature
50 reactivation of the anaphase promoting complex/cyclosome (APC/C) during G2 and allow
51 cells to bypass mitosis and enter G1 with tetraploid (4N) DNA content. Published work
52 shows that this M bypass largely requires p53 activation that in turn restricts continued
53 cell cycle progression[5,8]. Therefore, M bypass largely results in permanent cell cycle
54 arrest (i.e., senescence) when tetraploid cells are unable to re-enter S phase[6,8,9]. Since

55 the majority of cancers have mutated p53, and these cancers tend to be harder to
56 treat[10,11], and in light of a recent report that demonstrated p53-independent signals are
57 also involved in promoting M bypass[7], we sought to understand the cell cycle fates of
58 p53-deficient cancer cells that persist after genotoxic chemotherapy treatment.

59 Here, we confirm that p53-mutant cancer cells undergo widespread mitotic bypass
60 upon exposure to genotoxic chemotherapies. Interestingly, we find that the cells that
61 persisted after chemotherapy treatments did not undergo quiescence- or senescence-like
62 cell cycle arrest, but instead entered an endocycle and continued to undergo successive
63 rounds of genome duplication and mitotic bypass, ultimately becoming highly polyploid.
64 In these models, initial M bypass allows cells to evade chemo-induced mitotic
65 catastrophe, then continued endocycling shields DTPs from delayed cell death after drug
66 removal. In contrast to DTPs that reside in difficult to target states of cell cycle arrest, the
67 unique state of proliferative arrest but active cell cycle within the endocycle presents
68 opportunity for intervention. We find that persistent DNA damage in endocycling DTPs
69 makes them reliant on sustained G2 checkpoint signaling from WEE1 and Myt1, which
70 promotes continued M bypass and avoidance of mitotic catastrophe. Interestingly, the
71 roles of WEE1 and Myt1 are not redundant, and inhibiting either with a clinical-stage small
72 molecule inhibitor is sufficient to force mitotic catastrophe and cell death in endocycling
73 DTPs. Further, only Myt1 inhibition actively prevents M bypass, suggesting that Myt1
74 activity is required for premature APC/C reactivation. These results bolster previous
75 studies in demonstrating that canonical cell cycle commitment is readily reversed under
76 stress conditions, uncover the p53-independent drivers of this process, and define
77 endocycling persisters as a targetable reservoir of persistence after chemotherapy
78 treatment.

Results

Genotoxic chemotherapy induces widespread mitotic bypass

To monitor cell cycle dynamics in cancer cells responding to genotoxic stress, we engineered p53-mutant cancer cell lines PC3 (A138fs/del), DU145 (P223L/V274F), and MDA-MB-231 (R280K/R280K) to express the Ki67-T2A-FUCCI reporter[12]. The reporter utilizes an mCherry-Cdt1 degron and a mAG-Geminin degron to mark G1 and S/G2/M phases, respectively. The levels of each fluorescent reporter are controlled by APC/C activity, which directly degrades mAG-Geminin and indirectly leads to accumulation of mCherry-Cdt1[13] (**Fig. 1A,B**). Expression of the reporter is driven by the Ki67 promotor and therefore non-cycling Ki67$^-$ cells are identifiable as mCherry$^-$/mAG$^-$.

Timelapse imaging of FUCCI-expressing cells during treatment with LD_{50} doses of commonly used genotoxic drugs cisplatin, etoposide, and doxorubicin revealed that premature APC/C reactivation during chemo-induced G2 arrest was a widespread alternative to the expected cell cycle arrest, mitotic entry, and/or cell death (**Fig. 1C; S1A,B; and Supplementary Movie1**). These cells progress directly from G2 into tetraploid (4N) G1 without entering mitosis (no nuclear envelope breakdown or mitotic rounding), in line with previous reports of G2 cell cycle exit in response to various cellular stresses[5-7].

To quantify the frequency of mitotic bypass in the immediate response to chemotherapy, cells were treated for 72h with cisplatin, etoposide, or doxorubicin; drug was washed out and cells that survived 24h later were fixed and stained for endogenous geminin and DAPI (**Fig. 1D**). Fluorescence intensities were extracted from individually segmented nuclei to determine the cell cycle state of each cell (**Fig. S1C**). 56.7% of cisplatin-, 76.8% of etoposide-, and 68.1% of doxorubicin-treated PC3 had bypassed

103 mitosis, consistent with our observations in FUCCI imaging experiments (**Fig. 1E, S1D**).
104 Similarly, the majority of MDA-MB-231 and DU145 that survived etoposide or doxorubicin
105 treatment had bypassed mitosis, though cisplatin induced lower levels of bypass in these
106 cells (**Fig. S1E,F**). These data demonstrate that bypass of mitosis was a frequent event
107 in response to genotoxic chemotherapy in p53-mutant cancer cells. The prevalence of M
108 bypass in surviving cells suggests that this is an adaptive response in the presence of
109 genotoxic stress and is thereby selected for. Indeed, many cells that die in response to
110 these drugs do so after failing to maintain G2 arrest and undergoing mitotic catastrophe[14]
111 (**Fig. S1G**). Thus, M bypass s imparts a fitness advantage during chemotherapy treatment
112 by allowing damaged cells to circumvent mitotic cell death.
113

114 **Cells that persist after genotoxic chemotherapy enter a sustained endocycle**

115 Cell cycle arrest, whether reversible (exit into G0, quiescence) or permanent
116 (senescence), is a commonly reported fate of cells that survive initial chemotherapy
117 challenge[4,15-18]. Bypassing mitosis, a reported consequence of cellular stress, can trigger
118 permanent cell cycle exit (i.e., senescence)[9]. Here, however, despite proliferative arrest
119 and morphological similarities to classically senescent cells, virtually all surviving cells
120 remained Ki67^{+} and therefore continued to express the FUCCI reporter, demonstrating
121 that cell cycle arrest was rare. Instead, most surviving cells re-entered S phase after
122 chemo-induced M bypass. Of the PC3 that bypassed mitosis during treatment (**Fig**. **1E**,
123 red bars), 59.9% (cisplatin), 61.1% (etoposide), and 77.6% (doxorubicin), had re-entered
124 S phase and undergone endoreduplication (second round of genome duplication without
125 intervening mitosis), progressing past tetraploid (4N) G1 arrest (**Fig. 1E,** dark red bars).
126 Results were similar in MDA-MB-231 and DU145 (**Fig. S1E,F**) and suggest that neither

127 quiescence nor senescence were the primary cell fate after M bypass in surviving cells.
128 Just 24h after drug washout there were prominent 8N G1, 16N G2, and 16N G1
129 populations, which require cells to have undergone a second mitotic bypass (8NG1),
130 second endoreduplication (16NG2), and third mitotic bypass (16NG1), indicative of entry
131 into an endocycle (**Fig. S1D**). These data indicate that although surviving cells exhibited
132 the proliferative arrest and enlarged, flattened morphology that are hallmarks of
133 quiescence and/or classical senescence, these were not the primary cell fates after
134 chemotherapy challenge.

135 The drug doses used in these experiments result in 50% viability relative to
136 untreated controls after 72h treatment (i.e. LD_{50}), as described in the methods. In the days
137 following drug treatment and washout, cells continue to die such that by 5 days post-drug
138 washout, the surviving fraction is <10% of that at the end of treatment, as we have
139 described previously[19]. At this point 5 days post-treatment an average of 99.7%
140 (cisplatin), 99.7% (etoposide), and 99.8% (doxorubicin) of surviving PC3 had bypassed
141 mitosis, respectively, based on analysis of DNA content and geminin abundance (**Fig.**
142 **1F,G**). On average, only 0.9%, 1.1%, and 0.8% of these cells remained in a tetraploid
143 (4N) G1 state (i.e., mitotic bypass and subsequent arrest), confirming that endocycling
144 was far more common than cell cycle arrest in these surviving populations. Similarly,
145 92.9%, 85.2%, and 74.1% of MDA-MB-231 had bypassed mitosis 5 days-post treatment
146 with cisplatin, etoposide, or doxorubicin, respectively (**Fig. S2H**).

147 These persistent cells remained non-proliferative (no successful mitoses) for
148 several weeks after drug treatment but remained $Ki67^{+}$ and therefore continued to
149 express the FUCCI reporter. We observed active cell cycle progression in persistent cells
150 for the entire period of proliferative arrest after drug treatment, demonstrated by continued
151 FUCCI reporter oscillation during time-lapse imaging of PC3-FUCCI (**Fig. 1H;**

152 **Supplementary Movie2**). To confirm that FUCCI reporter oscillation accurately reported
153 cell cycle transitions through G1-S-G2, surviving cells were pulsed with 5-ethynyl-2'-
154 deoxyuridine (EdU) 1, 5, or 12 days after 72h cisplatin treatment and washout. Cells
155 incorporated EdU at each timepoint, confirming progression through S phase. Moreover,
156 discrete DNA content doublings continued over time after drug washout (**Fig. S1I**). Thus,
157 non-proliferative persistent cells continued to undergo whole-genome replication during
158 repeated endocycle S phases (endo-S), as the FUCCI imaging suggested.

159 Together, these data demonstrate that after surviving genotoxic drug treatment by
160 bypassing mitosis and avoiding mitotic cell death, persistent cells entered a sustained
161 endocycle: successive G1, S, and G2 phases followed by repeated M bypass (**Fig. 1I**).
162 Endocycling persisters (DTePs) make up the predominant surviving population after
163 treatment, demonstrating that the chemo-induced endocycle is an adaptive phenotype
164 that is strongly selected for after genotoxic damage. We therefore asked how M bypass
165 is controlled in these persistent cells, first during the acute response to chemotherapy
166 and then later during sustained endocycling after drug removal.

167

168 **CDK1 inhibition is sufficient to induce premature APC/C reactivation and**
169 **endocycling**

170 Chemo-induced mitotic bypass involves 1) inhibition of G2-M progression and 2)
171 premature APC/C reactivation during G2 arrest. Cyclin dependent kinase (CDK)1 activity
172 drives entry into mitosis. CDK1 inhibition arrests cells in G2 and in some cases can induce
173 premature APC/C activation and mitotic bypass[7,20-22]. We first asked whether CDK1
174 inhibition alone, in the absence of genotoxic stress, induced mitotic bypass and/or
175 endocycling in our models. FUCCI-expressing cell lines were treated with the CDK1

176 inhibitor Ro-3306[23] and imaged for 72h. CDK1i induced extensive APC/C reactivation
177 during G2 (mAG-geminin degradation) and mitotic bypass in all models tested. Most of
178 these cells proceeded to enter a subsequent S-phase (**Fig. 2A; S2A,B; and**
179 **Supplementary Movie3**). Geminin immunostaining of PC3 after 72h CDK1i treatment
180 confirmed that CDK1i alone induces widespread M bypass (>75% of cells) and
181 endoreplication (58.2% of cells), with cells reaching ploidies ≥32N (**Fig. 2B,C**). Similar
182 levels of endocycling occurred in MDA-MB-231 and DU145 after 72h CDK1i treatment
183 (**Fig. S2A,B**).

184 Multiple recent studies have demonstrated that CDK2 and CDK4/6 activities are
185 critical for preventing premature APC/C reactivation during G2[7,20,24], so we next tested
186 the roles of CDK2 and CDK4/6 activities in chemo-induced M bypass. In contrast to
187 CDK1i, neither CDK4/6 nor CDK2 inhibition induced appreciable mitotic bypass or
188 endoreplication in PC3 (**Fig. 2B,C**). If CDK2 and/or CDK4/6 activities prevent APC/C
189 reactivation during G2 arrest in chemo-treated cells, then inhibiting them during chemo-
190 induced G2 arrest would accelerate M bypass, as was shown previously in the context of
191 other stress conditions[7]. G2 arrest was induced by 24h treatment with cisplatin,
192 etoposide, or CDK1i (**Fig. 2B, S2C,D**) before adding CDK2i or CDK4/6i for 24h. Geminin
193 and DNA content were analyzed to quantify the levels of M bypass in each condition (**Fig**
194 **2D**).

195 In PC3, CDK2i alone induced low levels of bypass in unstressed, DMSO vehicle
196 controls and did not increase M bypass in response to cisplatin, etoposide, or CDK1i (**Fig.**
197 **2E**). Similar results were obtained in MDA-MB-231 (**Fig S2E**). CDK2, like CDK1, is a
198 target of DNA damage signaling and we reasoned that cisplatin or etoposide treatments
199 likely inhibit CDK2, rendering CDK2i treatment redundant. Indeed, WEE1-dependent
200 CDK2 phosphorylation (inhibition) is induced in both cisplatin- and etoposide-treated cells

201 (**Fig. S2F**). Since CDK2 is already inhibited by cisplatin- and etoposide-induced genotoxic
202 stress, the redundancy of adding a CDK2 inhibitor may explain its lack of effect in those
203 conditions, but its lack of effect in CDK1i-treated cells suggests that M bypass can
204 proceed even when CDK2 is active. Further studies will be needed to explain how chemo-
205 treated cells re-enter S phase after chemo-induced M bypass if CDK2 is inhibited, since
206 CDK2 is essential for this process in other models[21].

207 Inhibiting CDK4/6 during cisplatin-, etoposide-, or CDK1i- induced G2 arrest (**Fig.**
208 **2D**) only modestly increased the percent of cells that underwent M bypass in PC3 and
209 MDA-MB-231 (**Fig. 2E; S2E**). Unlike CDK2, CDK4/6 remains active under cisplatin and
210 etoposide treatment and continues to phosphorylate Rb in S and G2 cells regardless of
211 their ploidy (**Fig. S2G**). Therefore, the modest effect of CDK4/6 inhibition during G2 arrest
212 in these experiments suggests that premature APC/C reactivation occurs despite CDK4/6
213 activity in chemo-treated cells.

214 Taken together, these results demonstrate that CDK1 inhibition alone is sufficient
215 to induce widespread M bypass and endocycling, in agreement with a previous report[21].
216 The modest effect of CDK4/6i on levels of M bypass in stressed cells combined with the
217 widespread M bypass induced by CDK1i treatment alone suggests that chemo-induced
218 CDK1 inhibition itself is the major driver of G2 arrest and premature APC/C activation in
219 these stress conditions.

220

221 **WEE1-, Myt1- dependent CDK1 inhibition is required for drug-induced G2 arrest**
222 **and M bypass**

223 Inhibition of CDK1 is sufficient to induce M bypass and subsequent endocycling,
224 so we sought to determine the mechanism of chemo-induced CDK1 inhibition and
225 consequent M bypass in p53-mutant cells.

226 P53 and its effector p21 can induce M bypass in response to various cellular
227 stresses by inhibiting CDK1[6,25,26]. Despite being p53-mutant, we observe an increase in
228 p21 expression at both the mRNA and protein level in response to both cisplatin and
229 etoposide in our models (**Fig. S3A-D**). Upregulation of p21 protein appears to be cell
230 cycle phase-independent, with strong upregulation observed in surviving PC3 in all cell
231 cycle phases after 72h etoposide treatment (**Fig. S3E**). Because of its reported role in
232 mitotic bypass, we asked whether p53-independent p21 expression played a role in
233 mitotic bypass in our models. Inducible overexpression of p21 in PC3 (PC3-p21OE) was
234 not sufficient to induce mitotic bypass or endocycling (**Fig. S3F, G**). Further, p21
235 knockdown during etoposide treatment did not impair etoposide-induced M bypass or
236 endocycling. Thus, p21 does not appear to be critical for chemo-induced M bypass or
237 endocycling.

238 In the absence of functional p53, cell cycle arrest in G2 can be achieved through
239 inhibitory phosphorylation of CDK1 at T14 by Myt1 and at Y15 by WEE1[27,28]. CDC25
240 phosphatases remove these marks, thus CDK1 activity is controlled by the balance of
241 kinase and phosphatase activity, which are controlled by ataxia-telangiectasia mutated
242 (ATM) and/or ataxia-telangiectasia and Rad3-related (ATR) [29,30]. As expected, we
243 observed an increase in phosphorylation of both 11hosphor- sites on CDK1 in response
244 to cisplatin or etoposide in PC3, MDA-MB-231, and DU145, suggesting a role in mitotic
245 bypass (**Fig. S4A-C**). After 24h cisplatin or etoposide treatment, which induced CDK1
246 phosphorylation and G2 arrest (**Fig. S2B,C**), inhibition of either Myt1 or WEE1 kinases

247 was sufficient to reduce CDK1 phosphorylation on T14 or Y15, respectively. Inhibition of
248 ATR had a similar, though more modest effect, to that of inhibiting its effector kinase
249 WEE1 directly, while inhibiting ATM had no effect on CDK1 phosphorylation (**Fig. 3B**).
250 Thus, site-specific CDK1 phosphorylation is dependent on Myt1i and WEE1, and
251 inhibiting either individually is sufficient to reverse stress-induced CDK1 phosphorylation
252 in a site-specific manner, allowing us to individually assay the functional effects of these
253 phosphorylations on initial M bypass and subsequent endocycling.

254 If Myt1-dependent T14 phosphorylation or WEE1-dependent Y15 phosphorylation
255 are critical for initial chemo-induced M bypass, then inhibition during chemo-induced G2
256 arrest should lead to CDK1 reactivation, forcing mitotic entry, catastrophe and cell death.
257 Indeed, G2 checkpoint disruption is the premise that precipitated the development of both
258 Myt1 and WEE1 inhibitors for use in combination with DNA damaging agents for cancer
259 treatment[31-33]. Here, we sought to dissect the role of both kinases and their respective
260 CDK1 phosphorylation sites in chemo-induced mitotic bypass and cell survival. PC3-
261 FUCCI were treated as in (**Fig. 3A**) and time-lapse imaged for 24h following the addition
262 of inhibitors. The resulting time series images were used to annotate cell fates. Analysis
263 was limited to cells that were in G2 at the start of inhibitor treatment, which made up the
264 majority of cells in agreement with geminin and DNA content data (**Fig. S2B,C**). Six
265 distinct cell fates were observed in these experiments: successful mitoses, continued G2
266 arrest, cell death outside of mitosis, endo-mitosis (mitotic entry then exit before
267 karyokinesis, resulting in a 4N-G1 cell with an intact nucleus), mitotic bypass (mAG-
268 geminin degradation without mitotic entry), and mitotic catastrophe (either cell death
269 during mitosis or failed karyokinesis resulting in a single G1-like cell with highly
270 fragmented nuclei, which die within hours of mitotic failure) (**Fig. S4D**). Inhibition of Myt1,
271 WEE1, ATR, or ATM had little effect on the fates of unstressed, DMSO-treated controls,

272 and most cells completed successful mitoses (**Fig. 3C**). In G2 cells harboring damage
273 from cisplatin or etoposide treatment, the addition of WEE1, Myt1, or ATR inhibitors, which
274 disrupt CDK1 phosphorylation in a site-specific manner (**Fig. 3B**), forced widespread G2
275 checkpoint failure and mitotic catastrophe. ATM inhibition, which does not impair cisplatin-
276 or etoposide-induced CDK1 phosphorylation (**Fig. 3B**), did not negatively impact G2
277 arrest, mitotic bypass, or survival in these cells. The addition of a CDK1 inhibitor (CDK1i)
278 in combination with WEE1i, Myt1i, and ATRi completely reversed their effects
279 demonstrating that the results are dependent on CDK1 activity (**Fig. 3D,E**). Although
280 phosphorylation at either T14 or Y15 should prevent ATP binding and CDK1 activity, we
281 found that disrupting phosphorylation at either site is sufficient to induce widespread
282 CDK1 reactivation and mitotic catastrophe in stressed cells (**Fig. 3F**). Further, Myt1
283 inhibition consistently decreased cells' ability to bypass mitosis to a greater extent than
284 either WEE1i or ATRi (**Fig. S4E,F**), suggesting an as-yet unexplored requirement for Myt1
285 in stress-induced mitotic bypass. Thus, CDK1 phosphorylation- especially by Myt1-
286 controls M bypass and thereby promotes survival in response to genotoxic drugs. The
287 dependence of these cells on G2 checkpoint activity both highlights a well-known
288 vulnerability in DNA-damaged cells and demonstrates that these inhibitors (especially
289 Myt1i) also prevent stress-induced mitotic bypass. This vulnerability can be exploited to
290 prevent M bypass and instead force extensive mitotic catastrophe, dramatically reducing
291 the fraction of surviving cells after chemotherapy treatments, as previously described[31].
292

293 **WEE1, Myt1 activities are required for endocycling and survival in persistent cells**

294 CDK1 inhibition is an expected consequence of the acute stress response during
295 chemotherapy treatment, but persistent endocycling cells continued to bypass M long

296 after drug washout. Since we determined that WEE1 and Myt1 were critical for CDK1
297 inhibition, and that Myt1 was especially involved in mitotic bypass and survival in the
298 acute response to genotoxic drugs, we asked whether these kinases similarly affected
299 CDK1 phosphorylation and perpetuation of M bypass in endocycling persisters. In PC3
300 DtePs 1 or 8 days after cisplatin or etoposide treatment, inhibiting Myt1 or WEE1 strongly
301 decreased T14 or Y15 phosphorylation, respectively, suggesting their activities continue
302 to be required for CDK1 inhibition in endocycling persisters (**Fig. 4A; S5A**). To test the
303 functional consequences of disrupting this site-specific CDK1 phosphorylation in
304 endocycling persisters, PC3-FUCCI were treated with cisplatin for 3 days to induce
305 endocycling, drug was washed out, and endocycling cells that survived 4 days later were
306 treated with WEE1, Myt1, ATR, or ATM inhibitors and time-lapse imaged for 24h (**Fig. 4B**).
307 Six distinct cell fates were annotated, as in (**Fig. S4D**). Disrupting either T14 or Y15
308 phosphorylation with Myt1i or WEE1i, respectively, was sufficient to induce widespread
309 mitotic entry and catastrophe. ATRi had a similar effect to that of WEE1i, as expected
310 based on its role in activating WEE1 (**Fig. 4C**). While inhibition of either WEE1, Myt1, or
311 ATR induced widespread mitotic entry, only Myt1i reduced the fraction of cells that
312 underwent mitotic bypass, again demonstrating a specific dependence on Myt1 activity
313 for premature APC/C reactivation and mitotic bypass in DtePs (**Fig. 4D**). The effects of all
314 three inhibitors were reversed by adding CDK1i, so their effects on DteP cell fate are
315 directly related to their roles in CDK1 inhibition (**Fig. 4C**). ATM inhibition had no effect on
316 CDK1 phosphorylation (**Fig. S5B**) or on cell fate (**Fig. S5C**) in DtePs, demonstrating ATM-
317 independence as was seen in the acute response to drug.

318 Together, these data demonstrate that DtePs continue to have a specific
319 dependence on Myt1- and WEE1-dependent CDK1 inhibition to enforce the G2 DNA
320 damage checkpoint and promote their survival during the chemo-induced endocycle.

321 Interestingly, disruption of CDK1-Y15 phosphorylation via either WEE1i or ATRi did not
322 affect DtePs' ability to bypass mitosis, while disruption of CDK1-T14 phosphorylation via
323 Myt1i prevented mitotic bypass (**Fig. 4E**). These divergent responses, together with
324 previous data suggest a previously undescribed role for Myt1 in M bypass.
325

326 **Persistent DNA damage induces stress signaling during endocycle S phases**

327 Persistent G2 checkpoint activation after drug removal drives continued M bypass
328 in DtePs, but it was unclear what triggers CDK1 phosphorylation well after the acute
329 effects of genotoxic drugs. Polyploidy itself can induce DNA damage during S phase[34],
330 so we asked whether this was the case in DtePs. These cells do have higher levels of the
331 DNA double-strand break (DSB) marker γH2AX and related ATM/ATR activation
332 (phosphorylation of Chk1 and Chk2) compared to untreated cells (**Fig. 5A-F**). We
333 classified these cells as G1 or Post-G1 based on geminin abundance to evaluate whether
334 DNA damage and stress signaling were related to S phase entry, specifically. Levels of
335 DNA damage were similar in G1 and Post-G1 cells, so this damage is present prior to,
336 and is not induced as a direct consequence of endocycle S phase, in contrast to what
337 was found in a previous report[34] (**Fig. 5B**). Beyond their p53 mutations, there are no
338 described defects in DNA damage repair pathways in this model, and future studies will
339 be needed to understand the source of unresolved DNA damage in this context. In
340 contrast, levels of p-Chk1 and p-Chk2 were both higher in Post-G1 compared to G1 cells
341 (**Fig. 5D,F**). Therefore, we reasoned that persistent DNA damage is responsible for
342 inducing stress signaling during endocycle S phases, downstream CDK1 inhibition, and
343 perpetuation of M bypass in DtePs.

344 We next used CDK1i-induced endocycling cells (CDK1i-ECCs) as a tool to dissect
345 the roles of polyploidy vs. DNA damage in the activation of stress signaling during endo-
346 S phase, as 72h CDK1i treatment induces endocycling without inducing the high levels
347 of DNA damage seen after chemo treatments (**Fig. 5G,H**). We analyzed ATR and ATM
348 activation, as above, in CDK1-ECCs and found these cells had only slightly elevated
349 levels of p-Chk1 and p-Chk2, on average, and that levels were only slightly higher in post-
350 G1 compared to G1 cells (**Fig. 5I,J**). Thus, polyploidy alone is only sufficient to induce
351 low levels of S phase stress signaling. The modest increases in phosphorylation of Chk1
352 (1.01-fold increased) and Chk2 (1.63-fold increased) compared to that in cisplatin- (2.12-
353 and 3.58-fold increases in p-Chk1 and p-Chk2, respectively) or etoposide-treated (1.97-
354 and 2.17-fold increases in p-Chk1 and p-Chk2, respectively) endocycling persisters,
355 suggests that the presence of persistent DNA damage likely plays the dominant role in
356 driving endo-S phase stress signaling and persistent mitotic bypass in DtePs (**Fig. S6E**).
357 Thus, CDK1 inhibition and endocycling are triggered by genotoxic stress, then
358 endocycling induces further genotoxic stress and CDK1 inhibition in a circular loop that
359 maintains a continued endocycle in persister cells

360 **Discussion**

361 Chemotherapy tolerance and long-term persistence are critical drivers of cancer
362 progression and lethality. Our results show that M bypass resulting from premature APC/C
363 reactivation during genotoxic stress-induced G2 arrest is selected for in the presence of
364 widely used chemotherapeutics, allowing cells to circumvent the mitotic catastrophe and
365 cell death that these drugs induce. Stress-induced M bypass has been observed
366 previously in other models responding to various stresses[5-7]. Our results provide further
367 evidence that cell cycle commitment, once thought to be irreversible, is readily reversed
368 under stressed conditions.

369 CDK1 inhibition induced by genotoxic stress or by a specific CDK1 inhibitor is
370 sufficient to induce premature APC/C activation, mitotic bypass, and endocycling. CDK1
371 inhibition or genetic ablation is reported to induce endocycling in some, but not all models
372 (reviewed in [22]), together suggesting that caution should be taken in the development of
373 CDK1 inhibition as a therapeutic strategy. Though CDK1 inhibition alone may suppress
374 tumor growth, unintended WGD due to initiation of endocycling may exacerbate genome
375 instability and treatment resistance. Defining biomarkers to predict which cells may be
376 susceptible to CDK1i-induced endocycling would be an important consideration. Our
377 results further suggest that the combination of CDK1 inhibition with genotoxic agents, as
378 has been proposed for the treatment of metastatic pancreatic cancer[35], for example, may
379 be counterproductive, with CDK1 inhibition promoting M bypass and resistance to DNA
380 damage-induced cell death.

381 In contrast to the well-reported states of cell cycle arrest (i.e., quiescence or
382 senescence) that arise after chemotherapy treatment[4,15-18], persistent cells in our model
383 survive by accessing a sustained endocycle: a state of proliferative arrest but active cell
384 cycle where DNA replication is uncoupled from cell division, resulting in an increasingly

385 polyploid surviving population. Based on these results, it is likely that some previous
386 reports of therapy-induced quiescence or senescence may include populations of
387 endocycling cells, as has been suggested previously[36]. Future studies would benefit from
388 employing specialized tools such as a FUCCI or other cell cycle reporters to better define
389 "senescent" populations after drug treatment, since endocycling cells are distinct from
390 classically G0/G1 arrested senescent cells.

391 Polyploid cells are thought to be refractory to the effects of DNA damage due to
392 the protective effect of having multiple copies of each gene[37-46]. Previously published
393 studies largely focus on tetraploid cells, and it is unknown whether protection scales with
394 ploidy in the highly polyploid persister cells that we observe. Our data suggest that beyond
395 polyploidy itself, the route to polyploidy (i.e., the chemo-induced endocycle) shields cells
396 from the deleterious effects of chemotherapy and enables long-term persistence after
397 treatment.

398 Critically, their reliance on sustained G2 checkpoint signaling renders endocycling
399 persister cells vulnerable to inhibition of this checkpoint, namely by WEE1 and especially
400 Myt1 inhibitors. This vulnerability further distinguishes endocycling persisters from cells
401 that have undergone cell cycle arrest, as those cells reside in G1 or G0-like states and
402 therefore have no interaction with the G2 checkpoint. This vulnerability may be clinically
403 relevant since p53-mutated cancers that have undergone whole-genome doubling are
404 more refractory to treatment[47], but future studies are required to assess the relevance of
405 endocycling DTPs *in vivo*. Inhibition of WEE1 or Myt1 separately in either the acute chemo
406 response or in endocycling persister cells revealed that 1) disrupting phosphorylation at
407 either of the two inhibitory sites on CDK1 was sufficient to induce CDK1 reactivation, and
408 2) Myt1 inhibition but not WEE1 inhibition dramatically decreases the rate of M bypass,
409 suggesting that Myt1 activity may be required for M bypass. These differences in

410 response may be due to dfferences in protein localization (WEE1 is nuclear, while Myt1
411 acts on cytoplasmic CDK1), or on Myt1's kinase-independent role in CDK1 inhibition[48,49],
412 though further studies are needed define Myt1's role in cell cycle commitment and M
413 bypass in the context of DNA damage.

414 In summary, we demonstrate chemotherapy treatment commonly results in p53-
415 independent M bypass. Since p53-deficent cells are largely incapable of senescence
416 arrest, re-entry into S phase is common and triggers subsequent stress signaling, CDK1
417 inhibition, and prolonged endocycling. Cells that continue to endocycle preferentially
418 survive and the disruption of this cycle by targeting the WEE1- and Myt1-dependent G2
419 checkpoint forces widespread mitotic catastrophe and cell death.

420 **Materials and Methods**

421 **Cell culture**

422 PC3 (CRL-1435), MDA-MB-231 (CRM-HTB-26), DU145 (HTB-81), and HEK293T
423 (CRL-3216) were purchased from ATCC and cultured according to ATCC
424 recommendations. Flasks were passaged using TrypLE Express (Gibco #12604013)
425 when cells reached 60-80% confluence.

426

427 **Stable cell line engineering**

428 For FUCCI lines, 1.5e6 293T were plated in 10cm dishes. The following day, cells
429 were transfected for second generation lentivirus packaging as follows: 1ug of Hs.Ki67-
430 T2A-FUCCI plasmid (a gift from Alexander Zambon), 1ug of psPAX2:pMD2.G (both gifts
431 from Didier Trono, Addgene plasmid #12260, 12259) at an 8:1 ratio, and 5uL of X-
432 tremeGENE HP transfection reagent (Roche #6366244001) were combined in 200uL in
433 OptiMEM (Gibco 31985062) and incubated for 30 minutes before adding dropwise to
434 293T dishes. 18-20hr later, media was changed to target cell media + 30% heat
435 inactivated FBS. Packaging cells were allowed to condition media for 48hr before viral
436 harvest. Viral media was removed and filtered through a Millex HP 0.45um PES syringe
437 filter (Millipore SLHPM33RS). Lentivirus from 1-2 10cm dishes (10-20ml) was
438 concentrated using Clontech Lenti-X concentrator per manufacturer protocol (Takara
439 #631232). 350k target cells were plated per well of a 6-well plate. Following concentration,
440 viral pellet was resuspended in 2ml of target cell media + 30% heat inactivated FBS and
441 moved to target cells in 6 well plate. 10ug/ml Polybrene (Millipore TR-1003) was added
442 directly to well. Target cells were transduced for ~20hr before changing media. After 3
443 days recovery, cells were selected with 5ug/ml blasticidin (Gibco A1113903) until
444 untransduced control cells were dead.

445 For inducible p21 overexpression, Gateway donor pDONR223_CDKN1A_WT (a
446 gift from Jesse Boehm & William Hahn & David Root; Addgene plasmid # 82201) was
447 recombined with Gateway destination pLIX_403 (a gift from David Root; Addgene plasmid
448 # 41395) using Gateway LR Clonase II (Invitrogen #11791020) to generate the CDKN1A
449 expression clone.

450 For inducible p21 knockdown, Tet-pLKO-Neo[50] (a gift from Dmitri Wiederschain;
451 Addgene plasmid # 21916) [CITE] was digested with AgeI (New England Biolabs R3552)
452 and EcoR1 (New England Biolabs R3101), then scrambled or *CDKN1A*-targeting shRNA
453 were inserted using Instant Sticky-end Ligase Master Mix (New England Biolabs M0370)
454 all according to manufacturer's protocol.

455 Lentivirus packaging and PC3 transduction were carried out as above. 72 hours
456 later, Tet-pLKO-Neo cells were selected with 1mg/ml G418 and pLIX403-CDKN1A cells
457 were selected with 0.5μg/ml puromycin (pLIX403) until untransduced control cells were
458 dead. Expression of shRNAs or CDKN1A were induced by 1μg/ml doxycycline treatment
459 and knockdown/overexpression were confirmed by Western Blot.

460 <u>shRNA sequences:</u>

461 Scr:

462 CCGGGCGCGATAGCGCTAATAATTTCTCGAGAAATTATTAGCGCTATCGCGCTTTTT
463 G

464 sh*CDKN1A*:

465 CCGGCGCTCTACATCTTCTGCCTTACTCGAGTAAGGCAGAAGATGTAGAGCGTTTTT
466 G

467

468 **Drug treatments**

469 Each cell line was treated for 72 hours with increasing doses of cisplatin (Sigma
470 #232120), etoposide (Cell Signaling Technology #2200), or doxorubicin (Sigma #D1515)
471 and LD50 values were determined by Alamar Blue according to manufacturer's protocol
472 (Invitrogen #DAL1025). The following 72h LD50 values were used for each chemotherapy
473 drug treatment: PC3- 6μM cisplatin, 5μM etoposide, 200nM doxorubicin; MDA-MB-231-
474 12μM cisplatin, 6μM etoposide, 400nM doxorubicin; DU145- 2μM cisplatin, 1.5μM
475 etoposide, 50nM doxorubicin.
476 1μM WEE1i (Adavosertib, SelleckChem #S1525), 1μM Myt1i (RP-6306,
477 MedChemExpress #HY145817A), 1μM ATRi (Ceralasertib, #S7693), 1μM ATMi (KU-
478 60019, SelleckChem #S1570), 1μM CDK4/6i (Palbociclib, MedChemExpress
479 #HY50767), 500nM CDK2i (INX-315, SelleckChem #E1854), and 5μM CDK1i (Ro-3306,
480 SelleckChem #S7747) were used unless stated otherwise.
481
482 **Immunofluorescence Imaging and Cytometry analysis**
483 Cells were cultured in 8- or 12-well chamber slides (Ibidi #80841, 81202). Cells
484 were fixed in 4% paraformaldehyde for 15 minutes, then blocked and permeabilized with
485 0.3% Triton-X100 + 5% normal goat serum in PBS for 60 minutes. Primary antibody was
486 diluted in PBS containing 1% BSA and 0.3% Triton-X100 and cells were incubated with
487 primary antibody solution overnight at 4°C. After washing 3x 10min in PBS, fluorescent
488 secondary antibodies along with DAPI were diluted in the same antibody buffer, cells were
489 incubated for 60 minutes at room temperature, then washed 3x 10min in PBS before
490 mounting with Prolong Diamond antifade mounting medium (Invitrogen P36970).
491 Images were acquired using a Zeiss Observer Z1 microscope/ZEN pro 2.0 software (Carl
492 Zeiss Microscopy). Cytometry analysis was performed using CellProfiler and R. Briefly,

493 individual nuclei were segmented based on DAPI signal and intensity values within each
494 nucleus were extracted for each fluorescent channel using CellProfiler. Downstream
495 analysis and data visualization were performed using R.

496 Primary antibodies against p21 (#2947; 1:200), 23hosphor-Rb S807/11 (#8516;
497 1:5000), geminin (#52508; 1:1000), 23hosphor-Chk1 S345 (#2348; 1:50), and
498 23hosphor-Chk2 T68 (#2197; 1:100) were purchased from Cell Signaling Technologies.
499 Anti- geminin (ab104306; 1:25000) and γH2AX (ab22551; 1:10000) were purchased from
500 Abcam. Goat anti-mouse Alexa Fluor Plus 488 (A32723) or Alexa Fluor Plus 555
501 (A32727), and goat anti-rabbit Alexa Fluor Plus 488 (A32731) or Alexa Fluor Plus 555
502 (A32732) secondary antibodies were acquired from Invitrogen and used at 1:200.

503

504 **Immunoblotting**

505 Cells were scraped into ice-cold PBS and pelleted by centrifugation at 5000 x g for
506 5 minutes. Lysates were collected in RIPA supplemented with protease/phosphatase
507 inhibitors (Cell Signaling Technology #5872). Lysates were clarified by centrifugation at
508 10000 x g for 15 minutes at 4°C. Protein concentration was measured using Pierce BCA
509 assay (Thermo Scientific #23225) according to manufacturer protocol. Normalized
510 samples were mixed with 4x Laemmli buffer (BioRad #1610747) and boiled at 95°C for
511 10 minutes before being loaded into 4-20% Bis-tris polyacrylamide gels (BioRad
512 #4561095). Electrophoresis performed with Tris/Glycine/SDS buffer (BioRad #1610732).
513 Protein was transferred to nitrocellulose membranes (BioRad #1704158) using the
514 BioRad TransBlot Turbo system per manufacturer protocol. Membranes were blocked for
515 60 minutes in StartingBlock buffer (Thermo Scientific #37538). Primary antibody was
516 diluted in Intercept T20 buffer (Licor #927-65001) and membranes were incubated
517 overnight at 4°C with agitation followed by 3x 5min washes with TBST, then incubated 60

518 minutes in secondary antibody at room temperature, washed 3x 5min with TBST, and
519 imaged with Licor Odyssey imager. Primary antibodies against 24hosphor-CDK1 Y15
520 (#4539), CDK1 (#9116), p21 (#2947), and CDK2 (#18048) were purchased from Cell
521 Signaling Technology and used at 1:1000. Anti- 24hosphor-CDK T14 (#ab58509) and
522 24hosphor-CDK2 Y15 (ab314034) were purchased from Abcam and used at 1:1000. Anti-
523 actin (#A5441) was purchased from Sigma and used at 1:5000. Goat anti-Rabbit 800CW
524 (#926-32211) and goat anti-mouse 680RD (#926-68070) secondary antibodies were
525 purchased from Licor and used at 1:20000.
526
527 **Time lapse imaging**
528 Cells were plated in 96-well ImageLock plates (Sartorius #BA-04856) in phenol-
529 red free medium and imaged every 20 minutes with Incucyte SX5 equipped with
530 Green/Orange/NIR optical module (Sartorius).
531
532 **qPCR**
533 Cells were rinsed with ice-cold PBS then scraped into 1mL ice-cold PBS and
534 pelleted by centrifugation at 1000 x g for 5 minutes at 4°C. mRNA was isolated using
535 Rneasy Plus kit (Qiagen #74134) and concentration was quantified with NanoDrop One
536 (Thermo Scientific). Reverse transcription of 1ug input mRNA was done using iScript
537 cDNA synthesis kit (BioRad #1708890) according to manufacturer's protocol. Real-time
538 PCR was done using SssoFast EvaGreen (BioRad #1725200) and run on BioRad CFX
539 Opus real-time PCR machine. The following primers were purchased from Integrated
540 DNA technologies: CDKN1A (fwd: CGGAACAAGGAGTCAGACATT; rev:
541 AGTGCCAGGAAAGACAACTAC), ACTB (fwd: CATGTACGTTGCTATCCAGGC; rev:
542 CTCCTTAATGTCACGCACGAT).

543

544 **EdU incorporation assay**

545 Cells were plated in 8-well chamber slides (Ibidi #80841) and 24h later pulsed with
546 10uM EdU (Molecular Probes E10187) for 20h. Click-It Plus EdU assay (Molecular
547 Probes C10640) was performed according to manufacturer's protocol then samples were
548 incubated with DAPI for 10 minutes before mounting slides with Prolong Diamond
549 antifade mounting medium (Invitrogen P36970). Images were acquired and analyzed as
550 for Immunofluorescence experiments, above.

551

552 **Statistical analysis**

553 All statistical analyses were performed in R with α = 0.05. Specific comparisons, tests
554 used, and p values are described in each figure legend.

555 **Author contributions**

556 KT, KJP, and SRA designed the study; KT, LR, and MEY performed the experiments; KT,
557 LR, and GB analyzed the data, and KT wrote the manuscript with input from KJP and
558 SRA; KJP and SRA acquired funding.

559

560 **Acknowledgements**

561 We would like to thank Dr. Sergi Regot and Dr. Christina Ferrer for helpful discussion and
562 the current and former members of the Pienta and Amend groups for critical feedback.
563 This work was funded by US Department of Defense CDMRP/PCRP (W81XWH-20-
564 10353 and W81XWH-22-1-0680), the Prostate Cancer Foundation, and the Patrick C.
565 Walsh Prostate Cancer Research Fund to SRA; and NIH/NCI P01CA093900 and the
566 Prostate Cancer Foundation to KJP.

567

568 **Competing interests**

569 The authors declare no competing interests.

570

571 **Ethics**

572 All experiments were carried out using established human cell lines obtained from ATCC.
573 Cells lines were routinely tested for mycoplasma and identities were authenticated using
574 STR typing.

575 **References**

576 1. Marine, J.C., Dawson, S.J., and Dawson, M.A. (2020). Non-genetic mechanisms
577 of therapeutic resistance in cancer. Nat Rev Cancer *20*, 743-756.
578 10.1038/s41568-020-00302-4.
579 2. Pu, Y., Li, L., Peng, H., Liu, L., Heymann, D., Robert, C., Vallette, F., and Shen,
580 S. (2023). Drug-tolerant persister cells in cancer: the cutting edges and future
581 directions. Nat Rev Clin Oncol *20*, 799-813. 10.1038/s41571-023-00815-5.
582 3. Shen, S., Vagner, S., and Robert, C. (2020). Persistent Cancer Cells: The Deadly
583 Survivors. Cell *183*, 860-874. 10.1016/j.cell.2020.10.027.
584 4. Russo, M., Chen, M., Mariella, E., Peng, H., Rehman, S.K., Sancho, E., Sogari,
585 A., Toh, T.S., Balaban, N.Q., Batlle, E., et al. (2024). Cancer drug-tolerant
586 persister cells: from biological questions to clinical opportunities. Nat Rev Cancer
587 *24*, 694-717. 10.1038/s41568-024-00737-z.
588 5. Davoli, T., Denchi, E.L., and de Lange, T. (2010). Persistent telomere damage
589 induces bypass of mitosis and tetraploidy. Cell *141*, 81-93.
590 10.1016/j.cell.2010.01.031.
591 6. Zeng, J., Hills, S.A., Ozono, E., and Diffley, J.F.X. (2023). Cyclin E-induced
592 replicative stress drives p53-dependent whole-genome duplication. Cell *186*,
593 528-542 e514. 10.1016/j.cell.2022.12.036.
594 7. McKenney, C., Lendner, Y., Guerrero Zuniga, A., Sinha, N., Veresko, B., Aikin,
595 T.J., and Regot, S. (2024). CDK4/6 activity is required during G(2) arrest to
596 prevent stress-induced endoreplication. Science *384*, eadi2421.
597 10.1126/science.adi2421.

598 8. Ganem, N.J., and Pellman, D. (2007). Limiting the proliferation of polyploid cells.
599 Cell *131*, 437-440. 10.1016/j.cell.2007.10.024.
600 9. Johmura, Y., Shimada, M., Misaki, T., Naiki-Ito, A., Miyoshi, H., Motoyama, N.,
601 Ohtani, N., Hara, E., Nakamura, M., Morita, A., et al. (2014). Necessary and
602 sufficient role for a mitosis skip in senescence induction. Mol Cell *55*, 73-84.
603 10.1016/j.molcel.2014.05.003.
604 10. Zhou, X., Hao, Q., and Lu, H. (2019). Mutant p53 in cancer therapy-the barrier or
605 the path. J Mol Cell Biol *11*, 293-305. 10.1093/jmcb/mjy072.
606 11. Hientz, K., Mohr, A., Bhakta-Guha, D., and Efferth, T. (2017). The role of p53 in
607 cancer drug resistance and targeted chemotherapy. Oncotarget *8*, 8921-8946.
608 10.18632/oncotarget.13475.
609 12. Zambon, A.C., Hsu, T., Kim, S.E., Klinck, M., Stowe, J., Henderson, L.M., Singer,
610 D., Patam, L., Lim, C., McCulloch, A.D., et al. (2020). Methods and sensors for
611 functional genomic studies of cell-cycle transitions in single cells. Physiol
612 Genomics *52*, 468-477. 10.1152/physiolgenomics.00065.2020.
613 13. Peters, J.M. (2006). The anaphase promoting complex/cyclosome: a machine
614 designed to destroy. Nat Rev Mol Cell Biol *7*, 644-656. 10.1038/nrm1988.
615 14. Vakifahmetoglu, H., Olsson, M., and Zhivotovsky, B. (2008). Death through a
616 tragedy: mitotic catastrophe. Cell Death Differ *15*, 1153-1162.
617 10.1038/cdd.2008.47.
618 15. Guillon, J., Petit, C., Toutain, B., Guette, C., Lelievre, E., and Coqueret, O.
619 (2019). Chemotherapy-induced senescence, an adaptive mechanism driving
620 resistance and tumor heterogeneity. Cell Cycle *18*, 2385-2397.
621 10.1080/15384101.2019.1652047.

622 16. Duy, C., Li, M., Teater, M., Meydan, C., Garrett-Bakelman, F.E., Lee, T.C., Chin,
623 C.R., Durmaz, C., Kawabata, K.C., Dhimolea, E., et al. (2021). Chemotherapy
624 Induces Senescence-Like Resilient Cells Capable of Initiating AML Recurrence.
625 Cancer Discov *11*, 1542-1561. 10.1158/2159-8290.CD-20-1375.
626 17. Ashraf, H.M., Fernandez, B., and Spencer, S.L. (2023). The intensities of
627 canonical senescence biomarkers integrate the duration of cell-cycle withdrawal.
628 Nat Commun *14*, 4527. 10.1038/s41467-023-40132-0.
629 18. Fernandez, B., Passanisi, V.J., Ashraf, H.M., and Spencer, S.L. (2025). Single-
630 cell RNA sequencing reveals a quiescence-senescence continuum and distinct
631 senotypes following chemotherapy. Nat Commun *17*, 169. 10.1038/s41467-025-
632 66836-z.
633 19. Kim, C.J., Gonye, A.L., Truskowski, K., Lee, C.F., Cho, Y.K., Austin, R.H., Pienta,
634 K.J., and Amend, S.R. (2023). Nuclear morphology predicts cell survival to
635 cisplatin chemotherapy. Neoplasia *42*, 100906. 10.1016/j.neo.2023.100906.
636 20. Cornwell, J.A., Crncec, A., Afifi, M.M., Tang, K., Amin, R., and Cappell, S.D.
637 (2023). Loss of CDK4/6 activity in S/G2 phase leads to cell cycle reversal. Nature
638 *619*, 363-370. 10.1038/s41586-023-06274-3.
639 21. Ma, H.T., Tsang, Y.H., Marxer, M., and Poon, R.Y. (2009). Cyclin A2-cyclin-
640 dependent kinase 2 cooperates with the PLK1-SCFbeta-TrCP1-EMI1-anaphase-
641 promoting complex/cyclosome axis to promote genome reduplication in the
642 absence of mitosis. Mol Cell Biol *29*, 6500-6514. 10.1128/MCB.00669-09.
643 22. Porter, A.C. (2008). Preventing DNA over-replication: a Cdk perspective. Cell Div
644 *3*, 3. 10.1186/1747-1028-3-3.
645 23. Vassilev, L.T., Tovar, C., Chen, S., Knezevic, D., Zhao, X., Sun, H., Heimbrook,
646 D.C., and Chen, L. (2006). Selective small-molecule inhibitor reveals critical

647 mitotic functions of human CDK1. Proc Natl Acad Sci U S A *103*, 10660-10665.
648 10.1073/pnas.0600447103.
649 24. Kim, K., Armand, J., Kim, S., and Yang, H.W. (2025). E2F activity determines
650 mitosis versus whole-genome duplication in G2-arrested cells. Nat Commun *16*,
651 6677. 10.1038/s41467-025-62061-w.
652 25. Bates, S., Ryan, K.M., Phillips, A.C., and Vousden, K.H. (1998). Cell cycle arrest
653 and DNA endoreduplication following p21Waf1/Cip1 expression. Oncogene *17*,
654 1691-1703. 10.1038/sj.onc.1202104.
655 26. Ullah, Z., Lee, C.Y., and Depamphilis, M.L. (2009). Cip/Kip cyclin-dependent
656 protein kinase inhibitors and the road to polyploidy. Cell Div *4*, 10. 10.1186/1747-
657 1028-4-10.
658 27. Liu, F., Stanton, J.J., Wu, Z., and Piwnica-Worms, H. (1997). The human Myt1
659 kinase preferentially phosphorylates Cdc2 on threonine 14 and localizes to the
660 endoplasmic reticulum and Golgi complex. Mol Cell Biol *17*, 571-583.
661 10.1128/MCB.17.2.571.
662 28. Parker, L.L., Atherton-Fessler, S., and Piwnica-Worms, H. (1992). p107wee1 is a
663 dual-specificity kinase that phosphorylates p34cdc2 on tyrosine 15. Proc Natl
664 Acad Sci U S A *89*, 2917-2921. 10.1073/pnas.89.7.2917.
665 29. Boutros, R., Dozier, C., and Ducommun, B. (2006). The when and wheres of
666 CDC25 phosphatases. Curr Opin Cell Biol *18*, 185-191.
667 10.1016/j.ceb.2006.02.003.
668 30. Blackford, A.N., and Jackson, S.P. (2017). ATM, ATR, and DNA-PK: The Trinity at
669 the Heart of the DNA Damage Response. Mol Cell *66*, 801-817.
670 10.1016/j.molcel.2017.05.015.

671 31. Aarts, M., Sharpe, R., Garcia-Murillas, I., Gevensleben, H., Hurd, M.S.,
672 Shumway, S.D., Toniatti, C., Ashworth, A., and Turner, N.C. (2012). Forced
673 mitotic entry of S-phase cells as a therapeutic strategy induced by inhibition of
674 WEE1. Cancer Discov *2*, 524-539. 10.1158/2159-8290.CD-11-0320.
675 32. Hirai, H., Arai, T., Okada, M., Nishibata, T., Kobayashi, M., Sakai, N., Imagaki, K.,
676 Ohtani, J., Sakai, T., Yoshizumi, T., et al. (2010). MK-1775, a small molecule
677 Wee1 inhibitor, enhances anti-tumor efficacy of various DNA-damaging agents,
678 including 5-fluorouracil. Cancer Biol Ther *9*, 514-522. 10.4161/cbt.9.7.11115.
679 33. Szychowski, J., Papp, R., Dietrich, E., Liu, B., Vallee, F., Leclaire, M.E.,
680 Fourtounis, J., Martino, G., Perryman, A.L., Pau, V., et al. (2022). Discovery of an
681 Orally Bioavailable and Selective PKMYT1 Inhibitor, RP-6306. J Med Chem *65*,
682 10251-10284. 10.1021/acs.jmedchem.2c00552.
683 34. Gemble, S., Wardenaar, R., Keuper, K., Srivastava, N., Nano, M., Mace, A.S.,
684 Tijhuis, A.E., Bernhard, S.V., Spierings, D.C.J., Simon, A., et al. (2022). Genetic
685 instability from a single S phase after whole-genome duplication. Nature *604*,
686 146-151. 10.1038/s41586-022-04578-4.
687 35. Wang, Q., Bode, A.M., and Zhang, T. (2023). Targeting CDK1 in cancer:
688 mechanisms and implications. NPJ Precis Oncol *7*, 58. 10.1038/s41698-023-
689 00407-7.
690 36. Hayashi, K., Horisaka, K., Harada, Y., Ogawa, Y., Yamashita, T., Kitano, T.,
691 Wakita, M., Fukusumi, T., Inohara, H., Hara, E., and Matsumoto, T. (2024).
692 Polyploidy mitigates the impact of DNA damage while simultaneously bearing its
693 burden. Cell Death Discov *10*, 436. 10.1038/s41420-024-02206-w.

694 37. Darmasaputra, G.S., van Rijnberk, L.M., and Galli, M. (2024). Functional
695 consequences of somatic polyploidy in development. Development *151*.
696 10.1242/dev.202392.
697 38. Dewhurst, S.M., McGranahan, N., Burrell, R.A., Rowan, A.J., Gronroos, E.,
698 Endesfelder, D., Joshi, T., Mouradov, D., Gibbs, P., Ward, R.L., et al. (2014).
699 Tolerance of whole-genome doubling propagates chromosomal instability and
700 accelerates cancer genome evolution. Cancer Discov *4*, 175-185. 10.1158/2159-
701 8290.CD-13-0285.
702 39. Hassel, C., Zhang, B., Dixon, M., and Calvi, B.R. (2014). Induction of endocycles
703 represses apoptosis independently of differentiation and predisposes cells to
704 genome instability. Development *141*, 112-123. 10.1242/dev.098871.
705 40. Kuznetsova, A.Y., Seget, K., Moeller, G.K., de Pagter, M.S., de Roos, J.A.,
706 Durrbaum, M., Kuffer, C., Muller, S., Zaman, G.J., Kloosterman, W.P., and
707 Storchova, Z. (2015). Chromosomal instability, tolerance of mitotic errors and
708 multidrug resistance are promoted by tetraploidization in human cells. Cell Cycle
709 *14*, 2810-2820. 10.1080/15384101.2015.1068482.
710 41. Lopez, S., Lim, E.L., Horswell, S., Haase, K., Huebner, A., Dietzen, M., Mourikis,
711 T.P., Watkins, T.B.K., Rowan, A., Dewhurst, S.M., et al. (2020). Interplay between
712 whole-genome doubling and the accumulation of deleterious alterations in cancer
713 evolution. Nat Genet *52*, 283-293. 10.1038/s41588-020-0584-7.
714 42. Schmidt, M.J., Naghdloo, A., Prabakar, R.K., Kamal, M., Cadaneanu, R.,
715 Garraway, I.P., Lewis, M., Aparicio, A., Zurita-Saavedra, A., Corn, P., et al. (2025).
716 Polyploid cancer cells reveal signatures of chemotherapy resistance. Oncogene
717 *44*, 439-449. 10.1038/s41388-024-03212-z.

718 43. Herriage, H.C., Huang, Y.T., and Calvi, B.R. (2024). The antagonistic relationship
719 between apoptosis and polyploidy in development and cancer. Semin Cell Dev
720 Biol *156*, 35-43. 10.1016/j.semcdb.2023.05.009.
721 44. Mehrotra, S., Maqbool, S.B., Kolpakas, A., Murnen, K., and Calvi, B.R. (2008).
722 Endocycling cells do not apoptose in response to DNA rereplication genotoxic
723 stress. Genes Dev *22*, 3158-3171. 10.1101/gad.1710208.
724 45. Zheng, L., Dai, H., Zhou, M., Li, X., Liu, C., Guo, Z., Wu, X., Wu, J., Wang, C.,
725 Zhong, J., et al. (2012). Polyploid cells rewire DNA damage response networks to
726 overcome replication stress-induced barriers for tumour progression. Nat
727 Commun *3*, 815. 10.1038/ncomms1825.
728 46. Shu, Z., Row, S., and Deng, W.M. (2018). Endoreplication: The Good, the Bad,
729 and the Ugly. Trends Cell Biol *28*, 465-474. 10.1016/j.tcb.2018.02.006.
730 47. Hobor, S., Al Bakir, M., Hiley, C.T., Skrzypski, M., Frankell, A.M., Bakker, B.,
731 Watkins, T.B.K., Markovets, A., Dry, J.R., Brown, A.P., et al. (2024). Mixed
732 responses to targeted therapy driven by chromosomal instability through p53
733 dysfunction and genome doubling. Nat Commun *15*, 4871. 10.1038/s41467-024-
734 47606-9.
735 48. Liu, F., Rothblum-Oviatt, C., Ryan, C.E., and Piwnica-Worms, H. (1999).
736 Overproduction of human Myt1 kinase induces a G2 cell cycle delay by
737 interfering with the intracellular trafficking of Cdc2-cyclin B1 complexes. Mol Cell
738 Biol *19*, 5113-5123. 10.1128/MCB.19.7.5113.
739 49. Wells, N.J., Watanabe, N., Tokusumi, T., Jiang, W., Verdecia, M.A., and Hunter, T.
740 (1999). The C-terminal domain of the Cdc2 inhibitory kinase Myt1 interacts with
741 Cdc2 complexes and is required for inhibition of G(2)/M progression. J Cell Sci
742 *112 (Pt 19)*, 3361-3371. 10.1242/jcs.112.19.3361.

743 50. Wiederschain, D., Wee, S., Chen, L., Loo, A., Yang, G., Huang, A., Chen, Y.,
744 Caponigro, G., Yao, Y.M., Lengauer, C., et al. (2009). Single-vector inducible
745 lentiviral RNAi system for oncology target validation. Cell Cycle *8*, 498-504.
746 10.4161/cc.8.3.7701.

747

748

Figure 1. Genotoxic therapy-induced mitotic bypass precipitates persistent endocycling

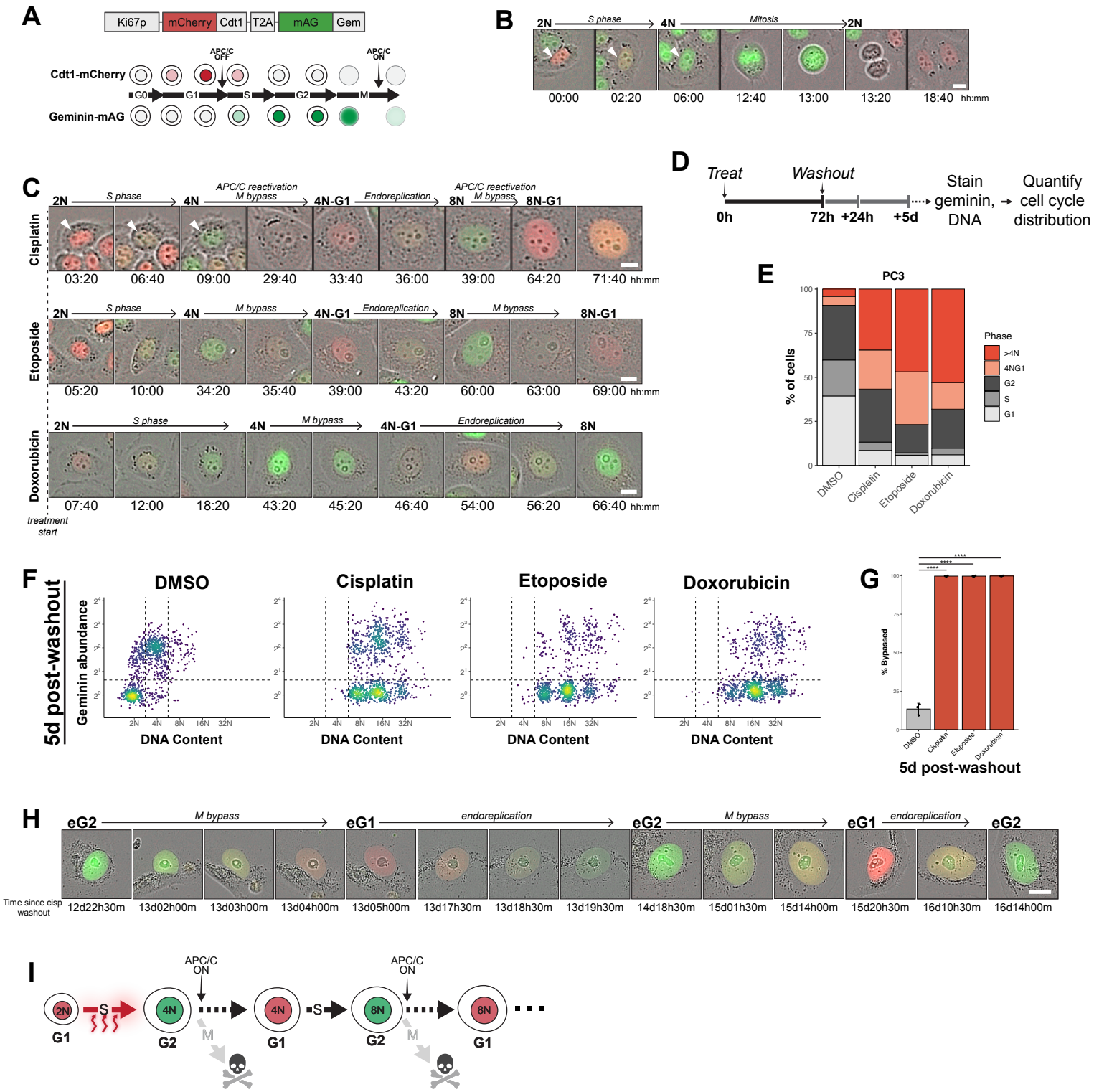

749 **Figure 1. Genotoxic therapy-induced mitotic bypass precipitates persistent**
750 **endocycling.**

751 **A.** Schematic of Ki67-T2A-FUCCI reporter and timeline of expression during cell cycle.

752 **B.** Representative time series shows reporter activity during a normal cell cycle in PC3-
753 FUCCI. Scale bar, 10μm.

754 **C.** Representative time series shows mitotic bypass and endoreplication in PC3-FUCCI
755 during 72h treatment with cisplatin, etoposide, or doxorubicin. Scale bar, 10μm.

756 **D.** Experimental outline for quantifying frequency of mitotic bypass after genotoxic
757 chemotherapy.

758 **E.** Quantification of percent of cells in each cell cycle phase in PC3 after treatment as in
759 (**D**). Data shown are mean percentages from 3 independent experiments.

760 **F.** Scatter plots of DNA content vs. geminin abundance in individual surviving PC3 5d
761 after 72h treatment with the indicated drugs. Points colored based on their relative
762 density. Dotted lines represent cut-off values for DNA content and geminin positivity.
763 Data shown are combined from 3 independent experiments.

764 **G.** Quantification of the percent of cells that had bypassed mitosis in (**F**). Data are mean
765 +/- sd from 3 independent experiments. p values calculated by one-way ANOVA and
766 Dunnett's post-hoc test comparing each treated condition to DMSO control. ****,
767 $p<0.0001$.

768 **H.** Representative time series of surviving PC3-FUCCI continuing to bypass mitosis and
769 endocycle >16 days after cisplatin treatment. eG1, endocycle-G1; eG2, endocycle-
770 G2. Scale bar, 20μm.

771 **I.** Model of protective effect of chemotherapy-induced premature APC/C reactivation
772 and continued endocycling. Colors of nuclei represent FUCCI reporter expression.

Figure 2. CDK1 inhibition is sufficient to induce premature APC/C reactivation and endocycling

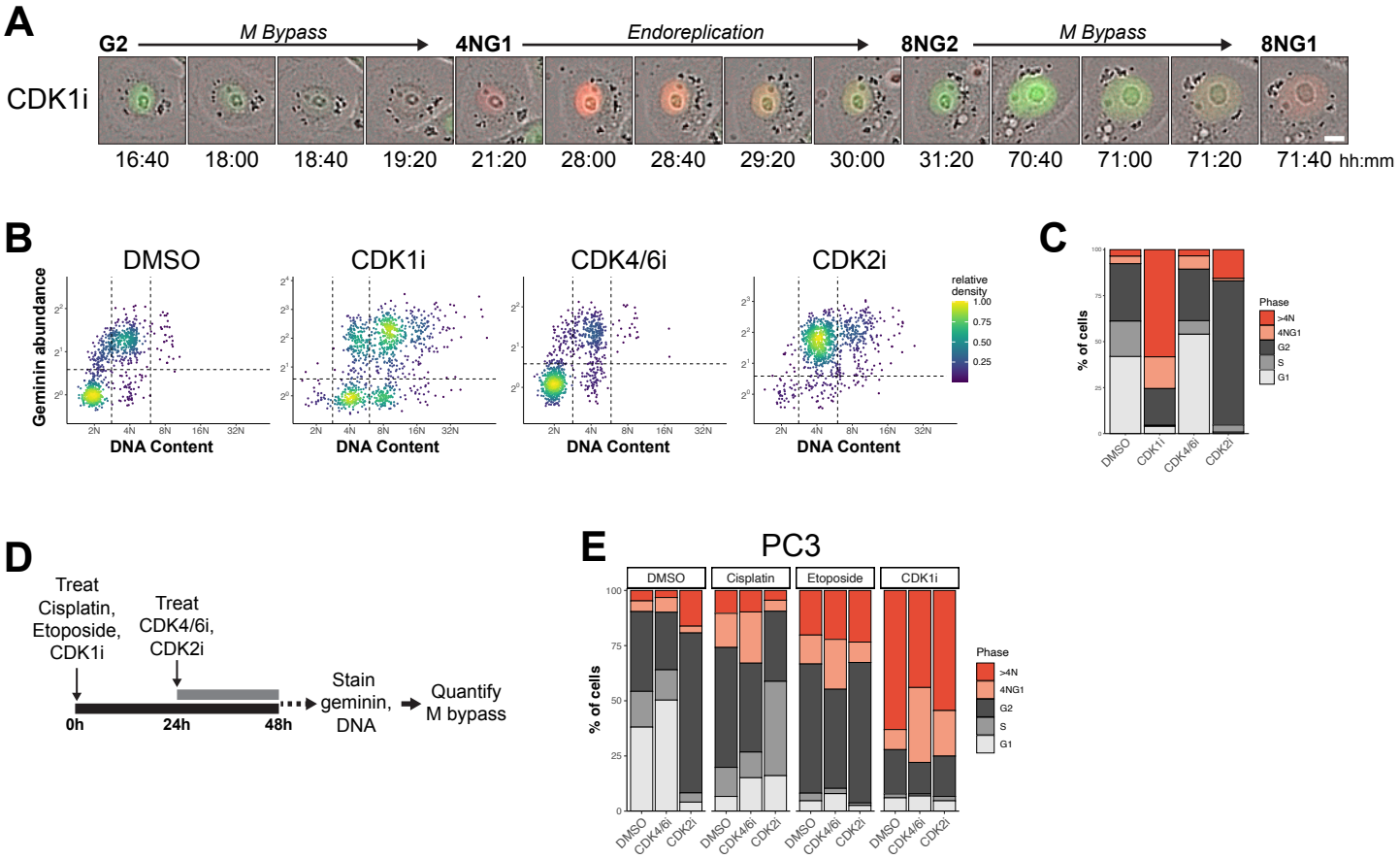

773 **Figure 2. CDK1 inhibition is sufficient to induce premature APC/C reactivation**
774 **and endocycling**

775 **A.** Representative time-lapse images of PC3-FUCCI undergoing mitotic bypass and
776 endoreplication during 72h treatment with CDK1i. Scale bar, 10μm.

777 **B.** Scatter plots of DNA content vs. geminin abundance in individual PC3 after 72h
778 treatment with DMSO, CDK1i, CDK4/6i, or CDK2i. Points colored based on their
779 relative density. Dotted lines represent cut-off values for determining DNA content and
780 geminin positivity. Data shown are combined from 3 independent experiments. 1000
781 individual nuclei shown for each condition.

782 **C.** Quantification of percent of cells in each cell cycle phase in each condition from (**B**).
783 Data shown are mean percentages from 3 independent experiments.

784 **D.** Experimental outline for determining the effects of CDK4/6i or CDK2i on cisplatin-,
785 etoposide-, or CDK1i- induced mitotic bypass.

786 **E.** Percent of PC3 in each cell cycle phase after treatment as in (**D**). Data shown are
787 mean percentages from ≥ 5 independent experiments.

Figure 3. WEE1-, Myt1- dependent CDK1 inhibition is required for G2 arrest and mitotic bypass

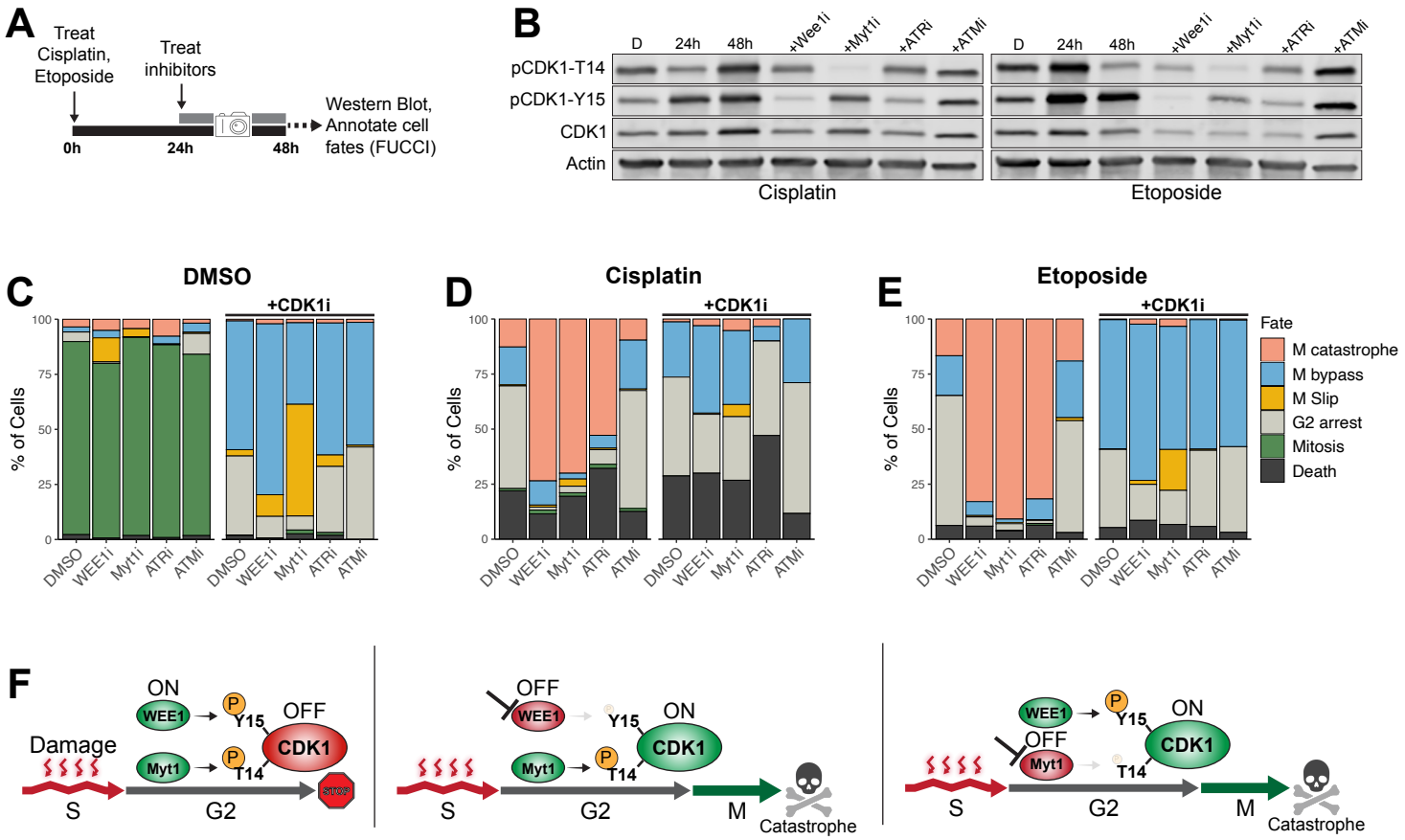

788 **Figure 3. WEE1-, Myt1- dependent CDK1 inhibition is required for drug-induced G2**
789 **arrest and M bypass**

790 **A.** Experimental outline for the analysis of the effects of WEE1, Myt1, ATR, or ATM
791 inhibition on cisplatin or etoposide-induced CDK1 phosphorylation and cell fate.
792 **B.** Western Blot of PC3 treated as in (**A**) showing the effects of WEE1i, Myt1i, ATRi, and
793 ATMi on cisplatin- or etoposide-induced CDK1 phosphorylation. D, DMSO.
794 **C-E.** Stacked bar plots showing the fates of PC3-FUCCI after DMSO (**D**), cisplatin (**E**), or
795 etoposide (**F**) +/- inhibitor treatments as depicted in (**A**). Data shown are the mean percent
796 of cells with each fate from ≥2 independent experiments.
797 **F.** Model of DNA damage-induced CDK1 inhibition (left) and the effects of WEE1 or
798 Myt1 inhibition (right).

Figure 4. WEE1, Myt1 activities are required for endocycling and survival in persistent cells

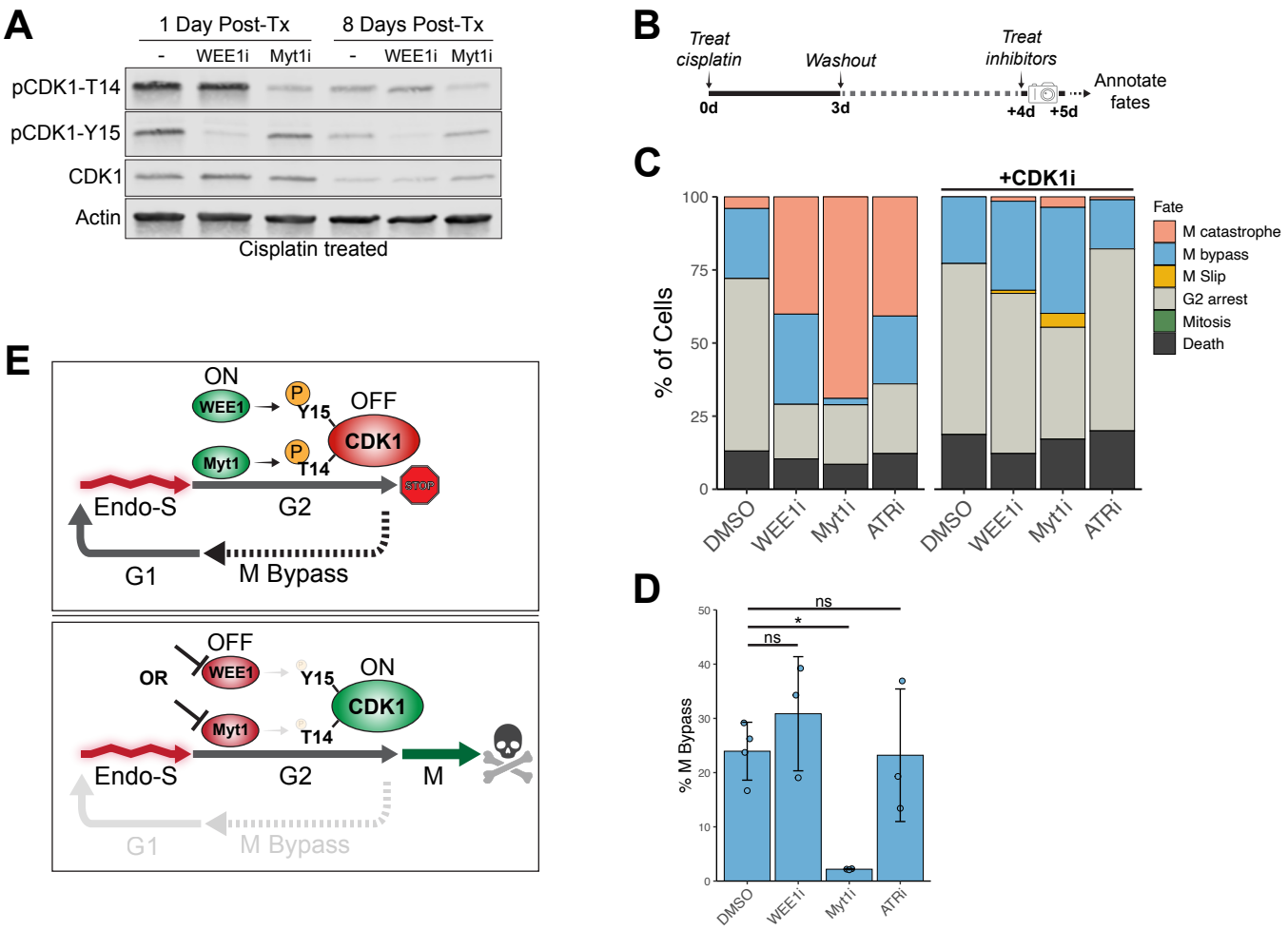

799 **Figure 4. WEE1, Myt1 activities are required for endocycling and survival in**
800 **persistent cells.**

801 **A.** Western Blot analysis of the effects of WEE1i or Myt1i on CDK1 phosphorylation in
802 DTePs 1- or 8-days post cisplatin treatment.

803 **B.** Experimental timeline for analysis of functional effects of WEE1i, Myt1i, ATRi, ATMi on
804 DTePs: PC3-FUCCI were treated for 3 days with cisplatin then drug was washed out.
805 4 days later, surviving cells were treated with WEE1i, Myt1i, ATRi, or ATMi +/- CDK1i
806 for 24 hours and timelapse imaged. Cell fates were then manually annotated.

807 **C.** Quantification of fates of PC3-FUCCI treated as in (**B**). Data shown are the mean
808 percent of cells with each fate from 3 individual experiments.

809 **D.** Quantification of % M bypass from (**C**). Data are mean +/- sd from ≥3 independent
810 experiments. p values calculated by one-way ANOVA and Dunnett's post-hoc test
811 comparing each treated condition to DMSO control. ns, not significant; *, $p<0.05$.

812 **E.** Model of control of M bypass in DTePs.

Figure 5. Persistent DNA damage induces stress signaling during endocycle S phases

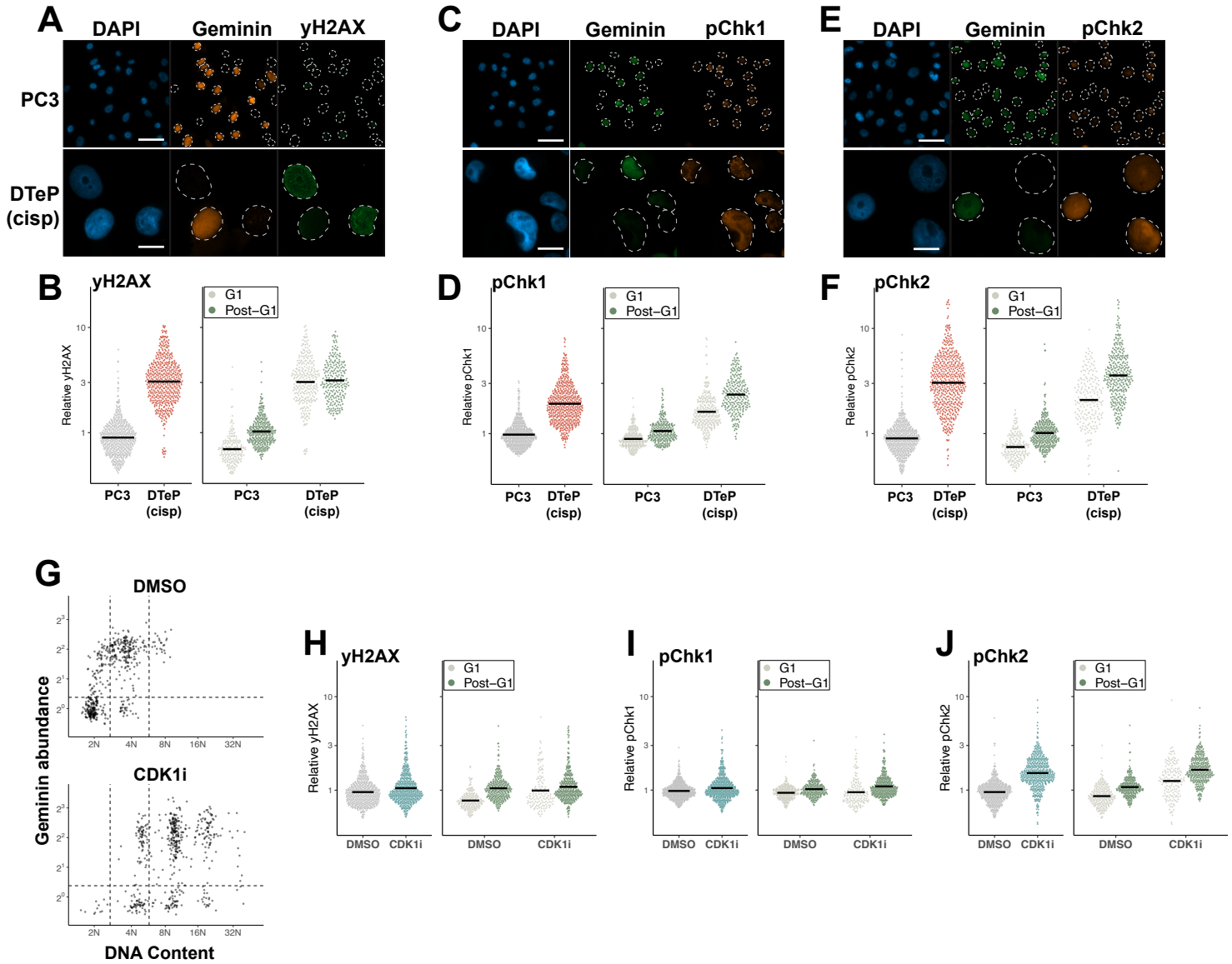

813 **Figure 5. Persistent DNA damage induces stress signaling during endocycle S**
814 **phases.**

815 **A.** Representative images of PC3 and DTePs 8 days post-cisplatin treatment co-
816 immunostained for geminin and yH2AX. Scale bar, 50μm.

817 **B.** Quantification of yH2AX abundance in individual nuclei from untreated PC3 and
818 DTePs 8 days post-cisplatin treatment (left) and same data with cells classified as G1
819 or post-G1 based on geminin abundance (right). Data are combined from 2
820 independent experiments. Mean for each group indicated by black line.

821 **C.** Representative images of PC3 and DTePs 8 days post-cisplatin treatment co-
822 immunostained for geminin and pChk1. Scale bar, 50μm.

823 **D.** Quantification of pChk1 abundance as in (**B**).

824 **E.** Representative images of PC3 DTePs 8 days post-cisplatin treatment co-
825 immunostained for geminin and pChk2. Scale bar, 50μm.

826 **F.** Quantification of pChk2 abundance as in (**B**).

827 **G.** Scatter plots of DNA content vs. geminin abundance in individual PC3 after 72h DMSO
828 or CDK1i treatment. Data are combined from 2 independent experiments, 500
829 individual nuclei shown per condition.

830 **H.** Quantification of yH2AX abundance in individual nuclei from PC3 treated 72h with
831 DMSO or CDK1i (left) and same data with cells classified as G1 or post-G1 based on
832 geminin abundance (right). Data are combined from 2 independent experiments, 500
833 individual nuclei shown per drug condition. Mean for each group indicated by black
834 line.

835 **I.** Quantification of pChk1 abundance in individual nuclei, as in (**H**).

836 **J.** Quantification of pChk2 abundance in individual nuclei, as in (**H**).